catalysts

MDPI

*Article*

# Forming a Cu-Based Catalyst for Efficient Hydrogenation Conversion of Starch into Glucose

**Shenghua Zhu [1], Jue Li [1], Fuchang Cheng [1] and Jinghua Liang [2,*]**

[1] CIMC ENTECH, 95 Yangcun 3rd Road, Dachang Street, Jiangbei New District, Nanjing 210048, China; zhu.shenghua@cimc.com (S.Z.); li.jue@cimc.com (J.L.); cheng.fuchang@cimc.com (F.C.)
[2] College of Biotechnology and Pharmaceutical Engineering, Nanjing Tech University (Nanjing Tech), 30 South Puzhu Road, Nanjing 211816, China
* Correspondence: jhliang@njtech.edu.cn; Tel.: +86-13770598601

**Abstract:** A pellet-forming as-catalyst, $CuO/Al_2O_3$, was prepared by the precipitation–tablet molding method and characterized by the Brunner–Emmet–Teller (BET), X-ray diffraction (XRD), X-ray photoelectron spectroscopy (XPS), and scanning electron microscopy (SEM) techniques and TEM. The characterization results showed that the formed $CuO/Al_2O_3$ was in situ reduced to $Cu/Al_2O_3$ and $Cu_2O/Al_2O_3$ catalysts in the reaction system. The catalytic performance of catalyzing hydrogenation starch into glucose was investigated in an autoclave over $CuO/Al_2O_3$. The yield of glucose reached 83.16% at a temperature of 160 °C, a pressure of 1.8 MPa, a 100 g starch solution of 15 wt%, a catalyst dosage of 2.25%, a reaction time of 4 h, and a rotational speed of 630 r/min. The reusability of the catalyst was evaluated, and the glucose yield did not decrease obviously even after being reused for five consecutive cycles. Starch was converted into glucose through the synergistic action of $Cu^+$ and $Cu^0$ catalysis. This work is expected to provide valuable insights into the design of catalysts and the hydrogenation process for efficient starch hydrogenation.

**Keywords:** forming as-catalyst $CuO/Al_2O_3$; $Cu/Al_2O_3$ and $Cu_2O/Al_2O_3$; starch; catalytical hydrogenating; glucose



**Citation:** Zhu, S.; Li, J.; Cheng, F.; Liang, J. Forming a Cu-Based Catalyst for Efficient Hydrogenation Conversion of Starch into Glucose. *Catalysts* **2024**, *14*, 132. https://doi.org/10.3390/catal14020132

Academic Editor: Shihui Zou

Received: 13 January 2024
Revised: 1 February 2024
Accepted: 7 February 2024
Published: 8 February 2024



## 1. Introduction

The rapid development of industry has led to an exponential increase in energy demand. As fossil resources become increasingly scarce, crude oil prices continue to rise [1]. In order to alleviate the consumption of fossil raw materials and the deterioration of the environment, a large number of renewable biomass resources are used to produce various materials, fuels, and chemicals [2]. Biomass is a promising renewable resource, with carbohydrates as its main component. Converting carbohydrates into fuels and chemicals is one effective way to alleviate the energy crisis [3,4]. Therefore, the development of sustainable renewable resources has garnered much attention. Starch is a major component of various biomasses and is one of the most abundant renewable resources on Earth, and it can be used as a sustainable energy source [5]. Starch is widely present in cassava, potatoes, yams, taros, and rice, and it can be used to produce beer and in the sugar industry (glucose and maltose) [6]. Among the numerous platform compounds of biomass conversion, glucose is an important platform compound that can be further converted into downstream products such as fructose, 5-hydroxymethylfurfural, pyruvic acid, sorbitol, ethylene glycol, etc., and is widely used in industries such as chemicals, food, medicine, and energy [7–9]. Moreover, glucose is also widely used in the human body, fermentation, and food processing and is the main raw material for wine-making, pharmaceuticals, and chemical production [10]. Starch can be divided into amylose and amylopectin, with amylose being composed of about 400 1, 4-D-glucose polymers and amylopectin having about 4% branching through 1, 6-glycosidic bonds on the basis of 1, 4-D-glucose polymerization [11]. Hydrolyzing starch

to produce glucose mainly involves breaking the 1, 4-glycosidic bond or 1, 6-glycosidic bond within polymer molecules [12].

Currently, the main methods for preparing glucose from starch include enzymatic hydrolysis [13], acid hydrolysis [14], and supercritical water hydrolysis [15–17]. The enzymatic hydrolysis of starch catalyzed by glucose amylase is the most common and effective method in industrial applications. However, this method still has certain limitations because of its low efficiency in hydrolyzing α-1, 6 bonds, resulting in a long reaction cycle [18]. Acid hydrolysis is an efficient method for glucose production, but it requires a large amount of acid and alkali in the refining process, which burdens subsequent wastewater treatment. On the other hand, the catalytic hydrogenation of starch to produce glucose can reduce the need for acid and alkali treatments [19]. In the experiments conducted by Wang et al. [20], the influence of ultrasound on starch hydrolysis during different stages of enzymatic hydrolysis was studied. It was found that using ultrasound treatments minimized enzyme activity loss and significantly improved the reaction rate. However, the use of ultrasound is expensive and increases costs. Vijay et al. [21] used activated carbon-supported tungstosilicic acid as a catalyst for starch hydrolysis and demonstrated the selectivity of glucose production through hydrothermal methods. No byproducts, such as pyruvic acid and formic acid, were produced during the experiment. Even after five consecutive reactions, the catalyst maintained its activity and selectivity without significant loss. However, the subsequent neutralization caused by acid catalyst immersion is environmentally undesirable. Therefore, considering a more efficient and economical method to promote the glycosylation reaction is a worthwhile research direction. The direct catalytic hydrogenation of biomass derivatives provides a simple operation method where, after the reaction, the catalyst can be filtered for reuse, reducing environmental pollution caused by acid and alkali neutralization. This process offers new insights into the production of various platform compounds from biomass [22].

Transition metal oxides are widely used as inexpensive and environmentally friendly catalysts in industrial catalysis [23]. The solvent for catalytic hydrogenation using metal oxide catalysts is water, which does not require disposal. Currently, precious metal catalysts such as Pt, Ru, and Pb have demonstrated excellent hydrogenation activity and selectivity. However, researchers have been striving to develop affordable and readily available non-precious metal hydrogenation catalysts. It has been discovered that inexpensive copper (Cu)-based catalysts [24,25] exhibit good performance in breaking C-O bonds and demonstrate excellent catalytic selectivity [26,27]. Because of their low cost and excellent catalytic performance, Cu-based catalysts have become a focus of research in the methanol oxidation carbonylation reaction [28,29]. However, there is relatively little research on the use of CuO for biomass degradation. In this context, Yang et al. [30], from our research group, studied the use of CuO as a catalyst for cellulose degradation to produce glucose. In this study, a $CuO/Al_2O_3$ as-catalyst was prepared using a precipitation-tableting method, and its catalytic performance in starch hydrogenation meant to produce glucose was investigated.

## 2. Results and Discussion

### *2.1. Crystallinity and Textural Properties*

The crystallinity of the resulting samples can be determined with powder XRD measurements. As shown in Figure 1a, the diffraction peaks at 2θ = 32.4°, 34.6°, 39.1°, and 57.7° are ascribed to the (110), (002), (200), and (202) planes of CuO (JCPDS 05-0661), respectively. It is worth noting that $Cu/Al_2O_3$ was produced via reduction from $CuO/Al_2O_3$ in situ, while the XRD diffraction peaks around 43.3°, 50.4°, and 74.1° correspond to the (111), (200), and (220) planes of Cu metal [31]. The diffraction peaks of Cu are in good agreement with JCPDS 04-0836, indicating the formation of Cu. It is worth noting that the diffraction peaks at 2θ = 29.55°, 36.4°, and 73.52° were detected, which are the same as the (110), (111), and (311) planes of $Cu_2O$ (JCPDS 05-0667), suggesting $Cu_2O$ is contained in $Cu/Al_2O_3$. Furthermore, for two samples, the typical characteristic peaks of $Al_2O_3$ can be

also observed; the diffraction peaks at 31.93° can be scripted to the (220) plane of γ-$Al_2O_3$, which is consistent with JCPDS 10-0425.

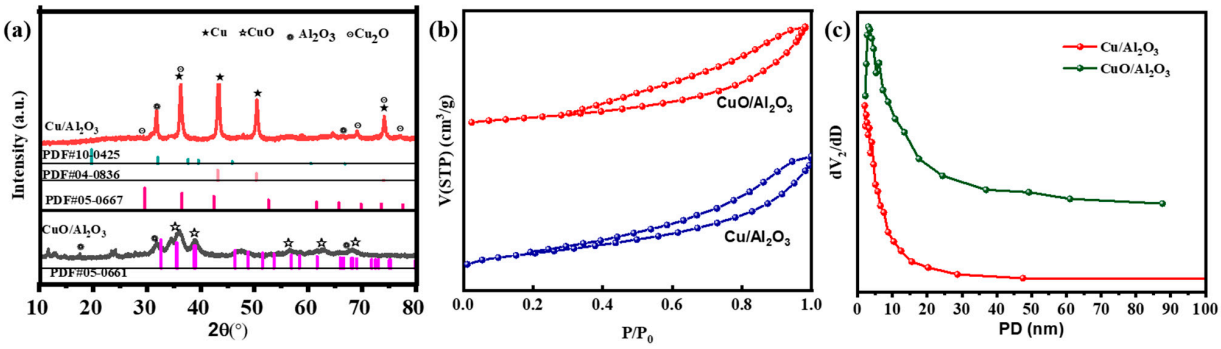


**Figure 1.** (**a**) XRD, (**b**) $N_2$-BET, and (**c**) pore size distribution patterns of $Cu/Al_2O_3$ and $CuO/Al_2O_3$.

The $N_2$ adsorption–desorption isotherms for the $CuO/Al_2O_3$ and $Cu/Al_2O_3$ solids are presented in Figure 1b. Two samples present type III isotherms according to the IUPAQ classification with a hysteresis loop of the $H_3$ type, indicating that the samples were in the presence of well-developed mesoporous structures with monolayer–multilayer adsorption and aggregates of plate-like particles, giving rise to slit-shaped pores [32]. The presence of mesoporous structures is further confirmed by pore size distribution curves in Figure 1c. The pore size distribution is relatively concentrated and mainly presents mesoporous structures. It can be seen from Table 1 that the specific surface area and pore volume of the Cu/A decreases significantly after reduction, from the initial 51.2 $m^2/g$ and 0.32 $m^3/g$ to 24.7 $m^2/g$ and 0.26 $m^3/g$, respectively, which can be attributed to the electrostatic action of Cu to make a part of the surface pores blocked [33].

**Table 1.** Specific surface area, pore size, and pore volume of Cu-based catalysts.

| Samples | $S_{BET}/(m^2/g)$ | $V_T/(cm^3/g)$ | Dpore/nm |
|---|---|---|---|
| $Cu/Al_2O_3$ | 24.7 | 0.26 | 7.9 |
| $CuO/Al_2O_3$ | 51.2 | 0.32 | 12.5 |

$S_{BET}$—BET surface area; $V_T$—total pore volume, dpore—average pore diameter, $P/P_0 = 0.992$.

### *2.2. Morphology and Microstructure*

In order to confirm the influence of the reduction process on the two samples, the morphologies of $CuO/Al_2O_3$ before and after reduction in situ via $H_2$ were investigated with TEM; the result is shown in Figure 2a,b. Before the reaction, the structure of the catalyst precursor, $CuO/Al_2O_3$, was loosely distributed, while the catalyst, $Cu/Al_2O_3$, is obviously aggregated after the reaction. This is because the catalyst precursor, $CuO/Al_2O_3$, was reduced by $H_2$ to form the catalyst, $Cu/Al_2O_3$, in situ, and the Cu dispersed on the surface of the $Al_2O_3$ carrier is gathered up because of electrostatic attraction between the metals. It can also be seen from the figure that the particle size of the catalyst decreases after reduction, which is in accordance with the conclusion of Figure 1c. The typical TEM micrograph and the particle size distribution histograms of CuO and Cu nanoparticles on the $Al_2O_3$ support are shown in Figure 2c,d, presenting a mean CuO particle size of 2.36 nm and a mean Cu particle size of 2.09 nm.

### *2.3. Surface Characterization of the Two Materials*

The XPS technique was used to investigate the surface chemical structure and Cu, Al, and O components of $CuO/Al_2O_3$, and the standard charge was calibrated using a C 1s binding energy of 284.8 eV. The results are shown in Figure 3. As depicted in Figure 3a, the presence of Cu (2p), Al (2p), and O (1s) was discovered by an XPS survey scan of the $CuO/Al_2O_3$ particles. Figure 3b shows the O 1s spectra. The O 1s spectra of the

$CuO/Al_2O_3$ as-catalyst were divided into three peaks using the Gauss decomposition method. According to a previous study [34], the lowest binding energy corresponds to lattice oxygen ($O_\alpha$) in mixed metal oxide, the medium binding energy is assigned to surface-adsorbed oxygen ($O_\beta$) species, and the highest binding energy is attributed to surface hydroxyl species ($O_\gamma$). Here, three peaks centering on 529.5 eV ($O_\alpha$), 531.0 eV ($O_\beta$), and 532 eV ($O_\gamma$) are assignable to lattice oxygen (Al-O, Cu-O), chemically adsorbed oxygen, and adsorbed water [35]. As depicted in Figure 3c, in the high-resolution XPS spectra of the Cu 2p core level of the reacted $CuO/Al_2O_3$ particles, the signal can be divided into five peaks at around 933.8 eV, 941.3 eV, 943.5 eV, 953.8 eV, and 962.2 eV [36]. According to the literature [37], the peaks of $Cu^{2+}$ detected at 933.7–934.1 eV and 953.4–954.8 eV on each sample can be assigned to Cu 2*p*3/2 and Cu 2*p*1/2, respectively. Here, representative peaks of Cu $2p_{3/2}$ (933.8 eV) and Cu $2p_{1/2}$ (953.8 eV) represent the CuO of Cu 2p. The characteristic $Cu^{2+}$ satellite peaks can be observed at 941.3 eV, 943.5 eV, and 962.2 eV, which are a result of hybridization between the 3d Cu orbital and the oxygen 2p orbital [38]. According to our previous study, the as-catalyst, $CuO/Al_2O_3$, was not detected in the presence of $Cu^+$, and only $Cu^{2+}$ formed on $CuO/Al_2O_3$ in the XPS analysis. The results were consistent with the results of XRD of $CuO/Al_2O_3$. Furthermore, as seen in Figure 3d, the Al 2p binding energy of $CuO/Al_2O_3$ was 74.5 eV, indicating Al (III) species [39].

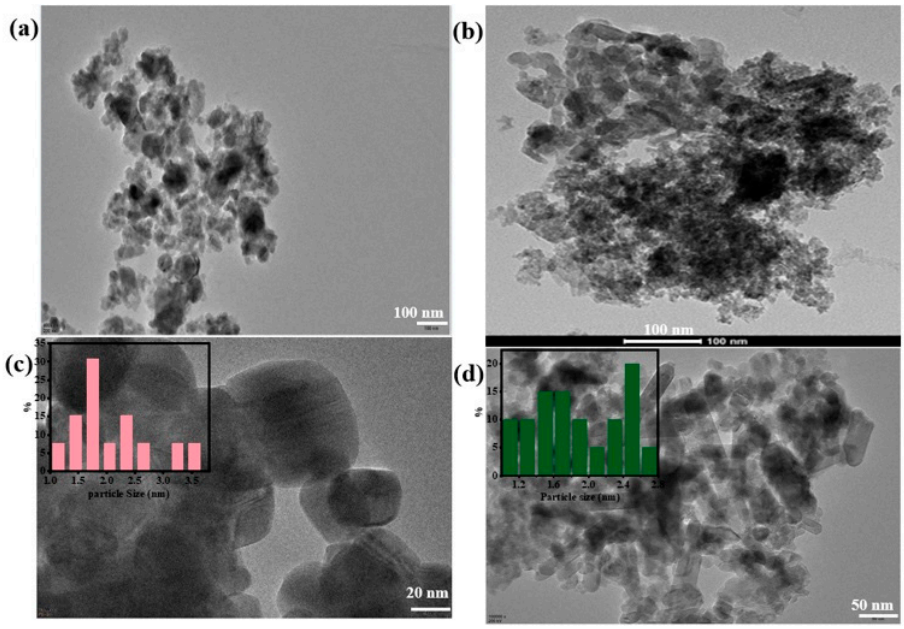


**Figure 2.** TEM image of (**a**,**c**) $CuO/Al_2O_3$ and (**b**,**d**) $Cu/Al_2O_3$.

After the hydrogenation reaction, the catalyst was characterized by XPS; the results are shown in Figure 4. As exhibited in Figure 4a, the compositions of the catalytical materials are still composed of three elements: Al, O, and Cu. Figure 4b shows the O 1 s spectra. The O 1 s spectra of the $Cu/Al_2O_3$ catalyst can be divided into three peaks by the Gauss decomposition method. Three peaks centering on 529.5 eV ($O_\alpha$), 531.0 eV ($O_\beta$), and 532 eV ($O_\gamma$) are assignable to lattice oxygen (Al-O, Cu-O), chemically adsorbed oxygen, and adsorbed water. However, it can be seen from the peak area that the lattice oxygen content was relatively reduced at this time, which may be due to the reduction of CuO into Cu and $Cu_2O$ caused by $H_2$ gas during the reaction. Furthermore, as shown in Figure 4c, the Al 2p binding energy of $Cu/Al_2O_3$ is about 74.5 eV, indicating that the valency of the $Al^{3+}$ species did not change. However, compared with Figure 3c, the bond energy of Cu in Figure 4d has changed. As shown in Figure 4d, two peaks centering on 932.0 eV and 951.8 eV are scripted to $Cu^0$ [40], which is consistent with XRD. The two peaks at 933.0 eV and 953.2 eV can be assignable to $Cu^+$ 2p3/2 and $Cu^+$ 2p1/2, respectively, indicating the

existence of $Cu^+$ in $Cu/Al_2O_3$. It is noteworthy that the active component of the catalyst that plays a catalytic role in the reaction is $Cu^0$ and $Cu^+$. The abundant $Cu^+$ species on the surface of the $Al_2O_3$ can effectively dissociate H from hydrogen [41]. Moreover, the $Cu^+$ species plays a remarkable role in polarizing the C–O bond, which can be effective in breaking the 1, 6-glucoside bond in starch.

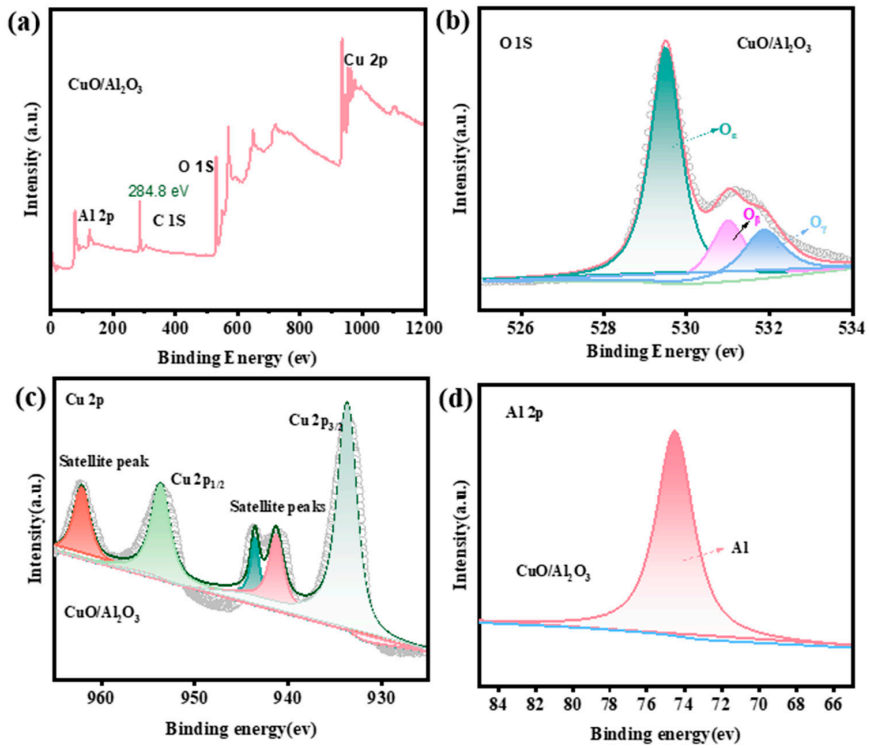


**Figure 3.** XPS spectra of (**a**) a full-range scan, (**b**) O 1s, (**c**) Cu 2p, and (**d**) Al 2p for the $CuO/Al_2O_3$.

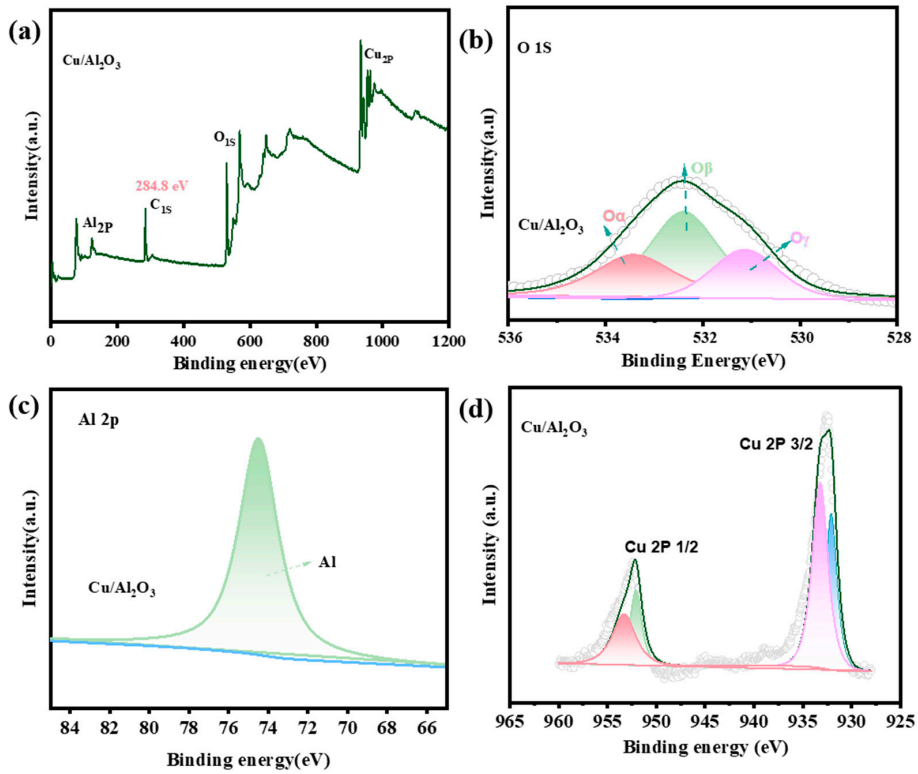


**Figure 4.** XPS spectra of (**a**) a full-range scan, (**b**) O 1s, (**c**) Al 2p, and (**d**) Cu 2p for the $Cu/Al_2O_3$.

### 2.4. Catalytic Activity

The catalytic activities of the resulting $Cu/Al_2O_3$ catalyst were evaluated for the hydrogenation of starch under a batch reactor. First, the influence of the reaction temperature in yielding glucose was investigated by proceeding with the reaction in a range of 140–170 °C under 1.8 MPa $H_2$, a rotation speed of 630 r/min, a 100 g starch solution of 15% (wt%), and a catalyst dosage of 2.25% for 4 h; the results were shown in Figure 5a.

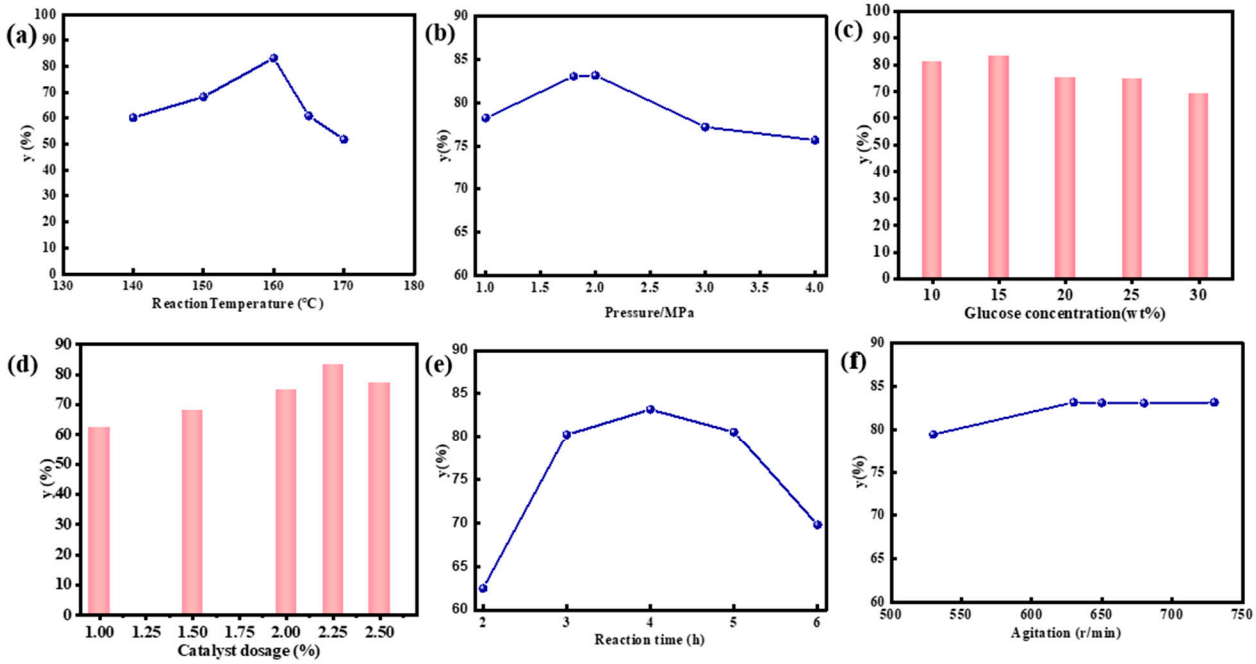


**Figure 5.** Glucose yield test with different conditions: (**a**) temperature, (**b**) pressure, (**c**) a starch solution concentration, (**d**) catalyst dosage, (**e**) reaction time, and (**f**) agitation.

As can be seen from Figure 5a, within a range of 140 °C to 160 °C, the glucose yield increases with the temperature. The highest glucose yield, 83.18%, was achieved at 160 °C. However, the glucose yield decreases with increasing reaction temperatures thereafter. This is because the starch solution and glucose solution will undergo coking at high temperatures, which can encapsulate the catalyst and cause it to lose activity because of coking, leading to a decrease in glucose yield. Therefore, the optimal temperature can be found at 160 °C for the subsequent optimization of starch hydrogenation.

Figure 5b illustrates the relationship between hydrogen pressure and glucose yield from 1 to 4 MPa at 160 °C, a rotation speed of 630 r/min, a 100 g starch solution of 15% (wt%), and a catalyst dosage of 2.25% for 4 h. As seen in Figure 5b, the glucose yield gradually increases with increasing pressure under a pressure range between 1 and 1.8 MPa. Under the conditions of 1.8 MPa and 2.0 MPa, the highest glucose yield, 83.18%, is achieved because of the optimal solubility of hydrogen in water and the resulting optimal catalytic effect. However, when the pressure reaches above 2.0 MPa, the hydrogen may continue to react with glucose to produce products such as glycerol, ethylene glycol, etc., resulting in a slight decrease in the yield of glucose with further a increase in reaction pressure. Therefore, an optimum pressure of 1.8 MPa was selected to investigate the other conditions.

To investigate the impact of starch concentration on catalytic reactions, we investigated the effect of starch concentration on glucose yield by using starch solutions with concentrations of 10, 15, 20, 25, and 30 wt% under reaction conditions of 160 °C, 1.8 MPa pressure, 630 r/min rotation speed, 4 h reaction time, and 2.25% catalyst dosage; the results are shown in Figure 5c.

As shown in Figure 5c, it can be observed that the glucose yield increases with the increase in starch concentration from 10% to 15%. An optimum glucose yield of 83.18% is

achieved using a 15% starch solution under hydrogenation conditions. However, when the starch concentration exceeds 15%, the glucose yield significantly decreases. This can be attributed to the fact that, within a certain range, an increase in starch concentration facilitates sufficient contact between starch and the catalyst, thereby benefiting the reaction process. However, excessively high concentrations result in the formation of multilayer starch adsorption on the catalyst surface during the reaction, leading to a decrease in the effective contact area and, consequently, a reduction in catalytic activity. Therefore, the optimal starch concentration under the experimental conditions is 15%.

The dosage of the catalyst also plays an important role in the starch hydrogenation reaction. The catalyst dosage varied between 1% and 2.5% (the mass of the catalyst divided by the total mass of starch and water is equal to the mass percentage of the catalyst), and its effect on the starch yield was studied. Reactions were performed under the same experimental conditions as above, that is a 160 °C reaction temperature, a 4 h reaction time, 630 r/min agitation speed, and a 100 g starch solution of 15 wt%. The further results are shown in Figure 5d.

As indicated in Figure 5d, the starch yield increases first and then decreases. In detail, a gradual increase in the starch yield is up to 83.18% when the catalyst dosage increases from 1% to 2.25%, which is probably due to more active sites resulting from the increase in the catalyst dosage. When the catalyst dosage increases from 2.25% to 2.5%, the decrease in the starch yield is small. On the one hand, too many catalysts are pushed together, and the effective active sites are relatively reduced, resulting in a decrease in catalytic efficiency. On the other hand, excess catalysts may hinder the adsorption and transformation of the product on the catalyst surface because of competitive adsorption. Consequently, the yield of the product is lowered. Therefore, taking all factors into consideration, especially the glucose yield, the optimal dosage of the catalyst is 2.25%.

In order to test the influence of reaction time, especially on the reaction pathway of starch hydrogenation, an experiment was carried out at 630 r/min with 1.8 MPa $H_2$ under the same conditions as above, that is, a 100 g starch solution (15 wt%), a 2.25% catalyst dosage, and a160 °C reaction temperature for reaction times ranging from 2 h to 6 h. The results are shown in Figure 5e. Based on the data presented in Figure 5e, it is evident that the glucose yield steadily increases as the reaction time extends from 2 to 4 h. The glucose yield reaches a maximum value of 83.18% when the reaction time is 4 h. However, beyond the 4 h mark, the glucose yield exhibits a noticeable decline, which indicates that a longer reaction duration does not necessarily result in a higher yield for starch hydrogenation. Within the first 4 h, starch can fully interact with the catalyst, leading to optimal reaction efficiency. However, as the reaction time exceeds 4 h, side products are generated during the reaction process, causing a decline in glucose yield. Therefore, the optimal reaction time is preferred to be 4 h.

The agitation rate also plays a critical role; especially in the solid–liquid–gas tri-phase reaction system, the mass transfer should not be ignored given the limited diffusion. Figure 5f illustrates the relationship between stirring rates and the glucose yield from 520 r/min to 730 r/min under the same conditions as above, that is, at a 160 °C reaction temperature, a 4 h reaction time, 1.8 MPa $H_2$, a catalyst dosage of 2.25%, and a 100 g starch solution of 15 wt%. As depicted in Figure 5f, the glucose yield rises to reach the required value after the agitation rate is more than 630 r/min. However, the potential risk and energy consumption should also be considered in this work. Therefore, the optimal reaction conditions can be set at 630 r/min.

### *2.5. Reusability and Supporter Comparison*

The reusability of $CuO/Al_2O_3$ was investigated with repeated use (five times) of the starch hydrogenation under the same reaction conditions as above, that is, at a 160 °C reaction temperature, a 4 h reaction time, 1.8 MPa $H_2$, a catalyst dosage of 2.25%, a 100 g starch solution of 15 wt%, and a 630 r/min agitation speed; the results are shown in Figure 6a. The 2.25 g catalyst amount used in the reusability studies remains unchanged,

which minimizes the influence of catalyst losses that may occur in the ultrasonic washing of the catalyst. After each cycle, the catalyst was filtered, washed with deionized water, and dried at 105 °C for 24 h. The recovery rate of the catalyst was over 90% because of a careful recycling operation. As seen in Figure 6a, no significant loss in glucose yield can be observed up to five times, which suggests that the catalytic activity remains stable and that this type of catalyst possesses a certain level of stability and potential industrial value.

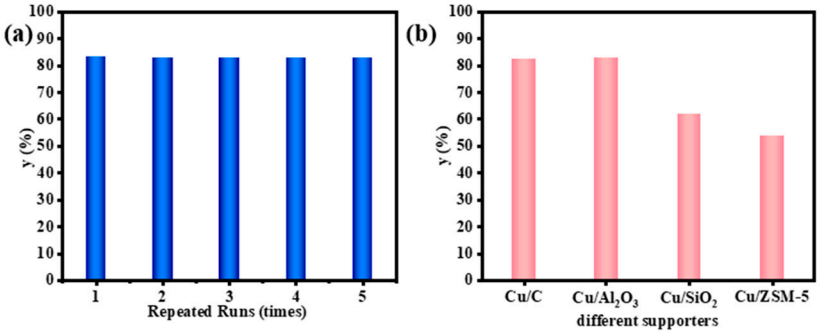


**Figure 6.** (**a**) Catalytic reusability of $Cu/Al_2O_3$; (**b**) effect comparison with different supports.

Moreover, some other supports, including active carbon, SiO2, and ZSM-5, were also selected to prepare the Cu catalysts in this work. The effect of catalysts prepared by these carriers on starch hydrogenation was investigated under optimized conditions (a 160 °C reaction temperature, a 4 h reaction time, 1.8 MPa $H_2$, a catalyst dosage of 2.25%, a 100 g starch solution of 15 wt%, and a 630 r/min agitation speed); the results are shown in Figure 6b. As exhibited in Figure 6b, under the same reaction conditions, $Cu/Al_2O_3$ was verified to be the best catalyst among all these different supporter catalysts.

## 3. Catalytic Mechanism Discussion

A simple Cu-based catalyst is a promising choice because of its high activity in the hydrogenolysis of C-O bonds, and it has already achieved high activity in the hydrogenolysis of glycerol [42]. Here, $Cu^0$ is essential as an active species for high catalytic activity. $Cu^0$ seems to be essential for high catalytic activity; however, the role of $Cu^{+1}$ cannot be excluded [32]. The active $Cu^+$ species of the catalyst polarize the C-O bonds and increase the activity of the catalyst for the hydrogenation of the C-O bond [43].

Based on the discussions above, we propose a possible reaction pathway, as shown in Scheme 1. The hydrolysis of starch into glucose can be considered two parallel reactions. In the presence of $H_2$, $CuO/Al_2O_3$ is reduced and converted into the active form of metallic $Cu^0/Al_2O_3$ and $Cu_2O$ at high temperatures. The active $Cu^0$ and $Cu_2O$ synergistically catalyze the hydrolysis of the C-O bond in the α-1, 4-glycosidic linkage of long-chain polysaccharides in starch. Meanwhile, in the hydrogenation of starch using water as a solvent, hot water molecules at the reaction temperature can produce acid in situ to act as the $H^+$ donor, which combines with the broken C-O bond to generate glucose [30]. In summary, the active $Cu^0$ and $Cu^+$ catalyze the hydrogenolysis of long-chain starch into low-molecular-weight glucose. The pH value of the reaction solution is acidic, and the theory of in situ acid production is valid because no additional acidic substances are added during the reaction. Therefore, under the synergistic effects of hydrothermal catalysis and $Cu^0$ and $Cu^+$ catalysis, starch is converted into glucose. Firstly, CuO is reduced to $Cu^0$ and $Cu_2O$ by $H_2$; then, it catalyzes the breaking cleavage of the C-O bond to generate glucose. At the same time, at the reaction temperature, hot water acts as the $H^+$ donor in the process of in situ acid production, which combines with the broken C-O bond to hydrolyze into low-molecular-weight glucose.

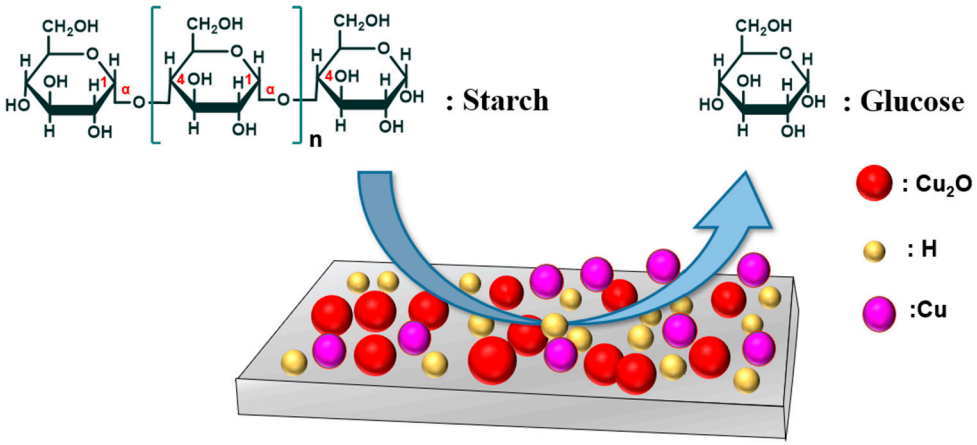


**Scheme 1.** The proposed hydrogenation route from starch to glucose, with $Cu/Al_2O_3$ pellets as catalysts.

## 4. Materials and Methods

### *4.1. Materials*

Soluble starch (AR) was acquired from Beijing Aoboxing Biotechnology Co., Ltd. (Beijing, China). $Cu(NO_3)_2.6H_2O$ (AR $\geq$ 99.5%) was purchased from Sinopharm Chemical Reagent (Shanghai, China). Boehmite (IR) was obtained from Dezhou Jinghuo Technology Co., Ltd. (Dezhou, China). Polyethylene glycol (PEG-4000) was purchased from Guangdong Guanghua Chemical Co., Ltd. (Guangdong, China). Deionized water was self-made, while aqueous ammonia (25 wt%) was obtained from National Pharmaceutical Group Chemical Reagent Co., Ltd. (Shanghai, China). Moreover, ultrahigh-purity $N_2$ (99.999%) and $H_2$ (99.999%) were both provided by Nanjing Special Gases (Nanjing, China). In addition, deionized water without carbon dioxide was used in all the experimental processes. The materials in this work were used without further purification.

### *4.2. Catalyst Preparation*

The active component of this catalyst is non-precious metal copper. The preparation process of the catalyst involved first taking a certain amount of copper nitrate and preparing a 3 mol/L aqueous solution in a three-mouth flask. Then, 25% aqueous ammonia was added to form Cu $(OH)_2$ precipitate, and the pH was maintained around 10 at 50 °C, followed by aging for 6 h. After vacuum filtration and washing, the precipitate was dried and put aside. Next, 30% copper hydroxide, 55% Boehmite, 10% polyethylene glycol, and 5% deionized water were mixed evenly and then pressed into shape by a press machine. The molded solid was placed in an oven and dried at 110 °C for 10 h. Finally, the molded solid was calcined in a muffle furnace at 500 °C for 4 h to obtain $CuO/Al_2O_3$.

### *4.3. Catalyst Characterization*

Textural properties were characterized through nitrogen sorption—desorption isotherms at −196 °C using a BK122W analyzer (JWGB Sci & Tech Ltd., Beijing, China). Before analysis, samples were degassed under vacuum for 6 h at 150 °C. The specific surface areas (SSAs) and porosity were achieved by calculations using the BET and BJH methods, respectively.

The morphology of the catalyst and the Ru NPs were measured with scanning electron microscopy (SEM) and transmission electron microscopy (TEM). Before testing, all of the samples were crushed into mesh-like powders via grinding in a crystal mortar. The SEM micrographs were acquired using a Hitachi S-4800 (Hitachi, Tokyo, Japan) electron microscope working at 200 kV.

The crystallinity of the samples after being crushed into mesh-like powders was determined by X-ray diffraction (XRD) patterns and recorded on a Rigaku Smartlab$^{TM}$ 9 Kw diffractometer (Rigaku, Osaka, Japan) equipped with Cu Kα radiation (λ = 1.542 Å)

operating at 40 kV and 100 mA in an angle range of 2θ = 5–60° with a step size of 0.03. To confirm the thermo-stability and CuO/γ-$Al_2O_3$ or Cu-based/γ- $Al_2O_3$ ratio of the resulting catalysts, an STA 449F3 thermogravimetric analyzer (TGA) (NETZSCH, Berlin, Germany) at a heating rate of 10 °C/min from 30 °C to 800 °C under $N_2$ flow was used in this work. Here especially, the samples were sealed with high-purity $N_2$ before being delivered for testing.

X-ray photoelectron spectroscopy (XPS) measurements of the crushed catalyst powders were performed with a K-Alpha spectrometer (Thermo Scientific, New York, NY, USA) with a monochromatic Al-Kα ray source under ultra-high vacuum conditions. In order to exclude external contamination, the samples were sealed with high-purity $N_2$ before being delivered for testing. Binding energy (BE) values were calibrated to the referenced C 1s peak (284.8 eV) during data processing of the XPS spectra. The peak decompositions assigned to the Cu 2p, Al 2p, and O 1s binding energy values were analyzed by applying mixed Gaussian–Lorentzian profiles and a Shirley nonlinear sigmoid-type baseline fitting of varying proportions (30–80%).

### *4.4. Catalytic Hydrogenation of Starch to Glucose*

The hydrogenation of starch was performed in a 150 mL stainless autoclave under vigorous stirring. In a typical reaction with 2% as-catalyst, 0.6 mL of formic acid, and 100 g of 15 wt% starch solution, the reactor was purged with hydrogen four times to remove air. The reactor was heated in a temperature range of 90–120 °C and then kept at the preset hydrogen pressure from 1 to 4 MPa. Here, the as-prepared Cu/$Al_2O_3$ precursor in the batch reactor was reduced in situ. During hydrogenation, the initial stirring rate was kept at the desired value (530–750 r/min). After the reaction, the solid catalyst was separated, washed, and dried under vacuum-drying at 60 °C for the next run. The residue solution was immediately filtered with a needle–drum membrane filter of 0.45 μm and analyzed via high-performance liquid chromatography (HPLC) (Shimadzu, Tokyo Japan) with refractive index (RI) detection. The HPLC column applied in this work was a SUGAR SC-1011 column (4.6 nm × 150 mm, Shodex, Tokyo, Japan) at 80 °C with a flow of 1 mL/min using deionized water as the mobile phase. Glucose yield was calculated using Equation (1), as follows:

$$y_{Glucose} = \frac{[\text{Glucose}]_f}{m} \times 100\% \quad (1)$$

where, $[\text{Glucose}]_f$ represents the final quality of glucose as detected, and m represents the initial quality of starch.

## 5. Conclusions

In summary, a CuO/$Al_2O_3$ catalyst was prepared via the precipitation-tableting method. XRD and XPS characterization confirmed the in situ reduction of CuO/$Al_2O_3$ into Cu/$Al_2O_3$ and $Cu_2O$/$Al_2O_3$. The hydrogenation process of starch to glucose over a Cu-based catalyst was investigated. Optimal reaction conditions were determined as follows: a temperature of 160 °C, a pressure of 1.8 MPa, a 100 g starch solution of 15 wt%, a catalyst dosage of 2.25%, a reaction time of 4 h, and a rotational speed of 630 r/min. Under these optimized conditions, the glucose yield reached 83.16%. Notably, the catalyst exhibited stable performance, showing no significant decrease in glucose yield even after being reused for five consecutive cycles. Starch was converted into glucose through synergistic actions, including $H^+$, $Cu^0$, and $Cu_2O$ catalysis. This work is expected to provide valuable insights into the design of catalyst and hydrogenation processes for efficient starch hydrogenation.

**Author Contributions:** Conceptualization, J.L. (Jinghua Liang); methodology, S.Z.; software, S.Z.; validation, J.L. (Jinghua Liang); investigation, J.L. (Jinghua Liang); data curation, S.Z.; writing—original draft, J.L. (Jue Li); writing—review and editing, J.L. (Jue Li) and F.C.; project administration, F.C. All authors have read and agreed to the published version of the manuscript.

**Funding:** This research received no external funding.

**Data Availability Statement:** All relevant data is included within the article.

**Conflicts of Interest:** Shenghua Zhu, Jue Li, and Fuchang Cheng are employed by CIMC ENTECH. The remaining authors declare that the research was conducted in the absence of any commercial or financial relationships that can be construed as potential conflicts of interest.

## References


1. Rasheed, T.; Anwar, M.; Ahmad, N.; Sher, F.; Khan, S.; Ahmad, A.; Khan, R.; Wazeer, I. Valorisation and Emerging Perspective of Biomass-Based Waste-to-Energy Technologies and their Socio-Environmental Impact: A Review. *J. Environ. Manag.* **2021**, *287*, 112257. [CrossRef] [PubMed]
2. Li, Z.; Wu, L.; Liu, C. Biomass Derived Bifunctional Catalyst for the Conversion of Cassava Dreg into Sorbitol. *Ind. Crop. Prod.* **2023**, *197*, 116493. [CrossRef]
3. Zelwicka, A.; Kolanowska, A.; Latos, P.; Jurczyk, S.; Boncel, S.; Chrobok, A. Carbon Nanotube/PTFE as a Hybrid Platform for Lipase B from Candida Antarctica in Transformation of A-Angelica Lactone into Alkyl-levulinates. *Catal. Sci. Technol.* **2020**, *10*, 3255–3264. [CrossRef]
4. Cheng, X.L.; Liu, Y.; Wang, K.; Yu, H.L.; Yu, S.T.; Liu, S.W. High-efficient Conversion of Cellulose to Levulinic Acid Catalyzed via Functional Brønsted–Lewis Acidic Ionic Liquids. *Catal. Lett.* **2022**, *152*, 1064–1075. [CrossRef]
5. Yepez, A.; Garcia, A.; Climent, M.S.; Romero, A.A.; Luque, R. Catalytic Conversion of Starch into Valuable Furan Derivatives Using Supported Metal Nanoparticles on Mesoporous Aluminosilicate Materials. *Catal. Sci. Technol.* **2014**, *4*, 428–434. [CrossRef]
6. Uchegbu, N.N.; Ude, C.F.; Nwadi, O.M.M. Optimisation of Enzymatic Fermented Glucose Production of Wild Cocoyam Starch Using Response Surface Methodology. *Glob. NEST J.* **2022**, *24*, 351–361.
7. Kang, S.; Fu, J.; Zhang, G. From Lignocellulosic Biomass to Levulinic Acid: A Review on Acid-Catalyzed Hydrolysis. *Renew. Sustain. Energy Rev.* **2018**, *94*, 340–362. [CrossRef]
8. Guo, Z.; Mao, J.; Zhang, Q.; Zhang, Q.L.; Xu, F. Integrated Biorefinery of Bamboo for Fermentable Sugars, Native-like Lignin, and Furfural Production by Novel Deep Eutectic Solvents Treatment. *Ind. Crop. Prod.* **2022**, *188*, 115453. [CrossRef]
9. Ba lachandran Kirali, A.; Sreekantan, S.; Marimuthu, B. Ce Promoted Cu/$\gamma$-$Al_2O_3$ Catalysts for the Enhanced Selectivity of 1,2-Propanediol from Catalytic Hydrogenolysis of Glucose. *Catal. Commun.* **2022**, *165*, 106447. [CrossRef]
10. Gallezot, P. Alternative Value Chains for Biomass Conversion to Chemicals. *Top. Catal.* **2010**, *53*, 1209–1213. [CrossRef]
11. Bušić, A.; Marđetko, N.; Kundas, S.; Morzak, G.; Belskaya, H.; Santek, M.I.; Komes, D.; Novak, S.; Santek, B. Bioethanol Production from Renewable Raw Materials and its Separation and Purification: A Review. *Food Technol. Biotechnol.* **2018**, *56*, 289–312. [CrossRef] [PubMed]
12. Mohsin, S.; Muhammad, S.; Qurratulann, A.; Ahmad, S.; Akhtar, M.W. Structural Engineering and Truncation of *A*-Amylase from the Hyperthermophilic Archaeon. *Methanocaldococcus Jannaschii. Int. J. Biol. Macromol.* **2024**, *256*, 128387.
13. Li, Z.; Cai, L.; Gu, Z.; Shi, Y. Effects of Granule Swelling on Starch Saccharification by Granular Starch Hydrolyzing Enzyme. *J. Agricul. Food Chem.* **2014**, *62*, 8114–8119. [CrossRef] [PubMed]
14. Intaramas, K.; Jonglertjunya, W.; Laosiripojana, N.; Sakdaronnarong, C. Selective Conversion of Cassava Mash to Glucose Using Solid Acid Catalysts by Sequential Solid State Mixed-Milling Reaction and Thermo-Hydrolysis. *Energy* **2018**, *149*, 837–847. [CrossRef]
15. Stummann, M.; Høj, M.; Gabrielsen, J.; Clausen, L.R.; Jensen, P.A.; Jensen, A.D. A Perspective on Catalytic Hydropyrolysis of Biomass. *Renew. Sustain. Energy Rev.* **2021**, *143*, 110960. [CrossRef]
16. Zhao, J.; Yang, X.; Wang, W.; Liang, J.H.; Orooji, Y.; Dai, C.; Fu, X.M.; Yang, Y.; Xu, W.L.; Zhu, J. Efficient Sorbitol Producing Process through Glucose Hydrogenation Catalyzed by Ru Supported Amino Poly (Styrene-Co-Maleic) Polymer (ASMA) Encapsulated on $\gamma$-$Al_2O_3$. *Catalysts* **2020**, *10*, 1068. [CrossRef]
17. Fu, X.; Ren, X.; Shen, J.; Jiang, Y.; Wang, Y.H.; Orooji, Y.; Xu, W.L.; Liang, J.H. Synergistic Catalytic Hydrogenation of Furfural to 1,2-Pentanediol and 1,5-Pentanediol with LDO Derived from Cumgal Hydrotalcite. *Mol. Catal.* **2021**, *499*, 111298–111305. [CrossRef]
18. Christina, Å.; Guido, Z.; Nelson, T.; Gorton, L. A Kinetic Model for Enzymatic Wheat Starch Saccharification. *Chem. Technol. Biotechnol.* **2000**, *75*, 306–314.
19. He, Z.; Zhang, L.; Gu, J.; Gu, J.; Pan, Q.; Zhou, S.; Gao, B.; Wei, D. Cloning of a Novel Thermostable Glucoamylase from Thermo Ph Ilic Fungus Rhizomucor Pusillus and High-Level Co-Expression with A-Amylase in Pichia Pastoris. *BMC Biotechnol.* **2014**, *14*, 114. [CrossRef]
20. Wang, D.; Hou, F.; Ma, X.; Chen, W.; Yan, L.; Ding, T.; Ye, X.; Liu, D. Study on the Mechanism of Ultrasound-Accelerated Enzymatic Hydrolysis of Starch: Analysis of Ultrasound Effect on Different Objects. *Int. J. Biol. Macromol.* **2020**, *148*, 493–500. [CrossRef]
21. Kumar, V.; Pulidindi, I.; Gedanken, A. Selective Conversion of Starch to Glucose Using Carbon Based Solid Acid Catalyst. *Renew. Energy* **2015**, *78*, 141–145. [CrossRef]
22. Manna, S.; Antonchick, A. Catalytic Transfer Hydrogenation Using Biomass as Hydrogen Source. *Chemsuschem* **2019**, *12*, 3094–3098. [CrossRef] [PubMed]

23. Cao, X.; Peng, X.; Sun, S.; Zhong, L.; Chen, W.; Wang, S.; Sun, R. Hydrothermal Conversion of Xylose, Glucose, and Cellulose under the Catalysis of Transition Mental Sulfates. *Carbohydr. Polym.* **2015**, *118*, 44–51. [CrossRef]
24. Xiang, Y.; Chitry, V.; Liddicoat, P.; Felfer, P.; Cairney, J.; Ringer, S.; Kruse, N. Long-Chain Terminal Alcohols through Catalytic CO Hydrogenation. *J. Am. Chem. Soc.* **2013**, *135*, 7114–7117. [CrossRef]
25. Chen, Q.; Meng, S.; Liu, R.; Zhai, X.H.; Wang, X.K.; Wang, L.; Guo, H.C.; Yi, Y.H. Plasma-Catalytic $CO_2$ Hydrogenation to Methanol over Cuo-Mgo/Beta Catalyst with High Selectivity. *Appl. Catal. B Environ.* **2024**, *342*, 123422. [CrossRef]
26. Mondal, S.; Malviya, H.; Biswas, P. Kinetic Modelling for the Hydrogenolysis of Bio-Glycerol in the Presence of a Highly Selective Cu-Ni-$Al_2O_3$ Catalyst in a Slurry Reactor. *React. Chem. Eng.* **2019**, *4*, 595–609. [CrossRef]
27. Oberhauser, W.; Evangelisti, C.; Jumde, R.; Psaro, R.; Vizza, F.; Bevilacqua, M.; Filippi, J.; Machado, B.F.; Serp, P. Platinum on Carbonaceous Supports for Glycerol Hydrogenolysis: Support Effect. *J. Catal.* **2015**, *325*, 111–117. [CrossRef]
28. Zhang, G.; Yan, J.; Wang, J.; Jia, D.S.; Zheng, H.Y.; Li, Z. Effect of Carbon Support on the Catalytic Performance of Cu-Based Nanoparticles for Oxidative Carbonylation of Methanol. *Appl. Surf. Sci.* **2018**, *455*, 696–704. [CrossRef]
29. Kabir, G.; Hameed, B. Recent Progress on Catalytic Pyrolysis of Lignocellulosic Biomass to Highgrade Bio-Oil and Bio-Chemicals. *Renew. Sustain. Energy Rev.* **2017**, *70*, 945–967. [CrossRef]
30. Yang, X.; Zhao, J.; Liang, J.; Zhu, J. Efficient and Selective Catalytic Conversion of Hemicellulose in Rice Straw by Metal Catalyst under Mild Conditions. *Sustainability* **2020**, *12*, 10601. [CrossRef]
31. Liu, Y.; Zhang, X.; Chen, L.; Liu, J.; Zhang, Q.; Ma, L. A Cu-ZnO-$Al_2O_3$ Catalyst with Oxygen Vacancy for Efficient Hydrodeoxygenation of Lignin-Derived Guaiacol to Hydrocarbons. *Chem. Eng. Sci.* **2024**, *285*, 119616. [CrossRef]
32. Shi, Y.; Ren, X.; Liu, B.Q.; Xu, S.; Zhang, H.; Gu, Y.; Xu, Y.; Lu, L.; Xu, W.; Liang, J. Ultrahigh Selectivity Self-Condensation of Cyclohexanone over $TiO_2/Al_2O_3$. *Catal. Kinet. Study* **2023**, *136*, 2071–2087. [CrossRef]
33. Yang, X.; Erickson, L.; Hohn, K.; Jeevanandam, P.; Klabunde, K.J. Sol-Gel Cu-$Al_2O_3$ Adsorbents for Selective Adsorption of Thiophene out of Hydrocarbon. *Ind. Eng. Chem. Res.* **2006**, *45*, 6169–6174. [CrossRef]
34. Ostovar, S.; Moussavi, G.; Mohammadi, S.; Marin, M.L.; Bosca, F.; Diego-Lopez, A.; Giannakis, S. Rapid Degradation of Omeprazole and Highly Effective Inactivation of *E. coli* in the UVA-light Photocatalytic Process with Cu-doped in Spinel-Structured ɣ-$Al_2O_3$ as a Stable Catalyst. *Chem. Eng. J.* **2024**, *479*, 147536. [CrossRef]
35. Wang, X.; Chong, J.; Liang, S.; Guo, M.; Zhang, M. Contributions of Mn-Doping in Cuo/$Al_2O_3$ Sorbent for Enhancement of $H_2S$ Removal at Low and Wide Temperature Range. *Fuel* **2023**, *334*, 126546. [CrossRef]
36. Zhang, X.; Gong, J.; Lin, B.; Zhou, Y. A Highly Atom-Efficient and Stable Copper Catalyst Loaded on Amorphous Uio-66-$NH_2$ for Hcl Oxidation to Chlorine. *Appl. Catal. A Gen.* **2022**, *634*, 118532. [CrossRef]
37. Wu, X.; Meng, H.; Du, Y.; Liu, J.; Hou, B.; Xie, X. Insight into $Cu_2O$/CuO Collaboration in the Selective Catalytic Reduction of NO with $NH_3$: Enhanced Activity and Synergistic Mechanism. *J. Catal.* **2020**, *384*, 72–87. [CrossRef]
38. Singh, R.; Kundu, K.; Pant, K.K. $CO_2$ Hydrogenation to Methanol over Cu-ZnO-$CeO_2$ Catalyst: Reaction Structure-Activity Relationship, Optimizing Ce and Zn Ratio, and Kinetic Study. *Chem. Eng. J.* **2024**, *479*, 147783. [CrossRef]
39. Yan, J.; Li, J.; Peng, J.; Zhang, H.; Zhang, Y.; Lai, B. Efficient Degradation of Sulfamethoxazole by the Cuo@$Al_2O_3$ (EPC) Coupled PMS System: Optimization, Degradation Pathways and Toxicity Evaluation. *Chem. Eng. J.* **2019**, *359*, 1097–1110. [CrossRef]
40. Zhou, C.; Lv, G.; Zou, X.; Wang, J.; Chen, Y.; Shen, J.; Su, S.; Xing, W.; Fan, D.; Shen, Y. Construction of Core-Shell Coordination Sponge-$Fe^0$@Cu-Pd Trimetal for High Efficient Activation of Room-Temperature Dissolved Ambient Oxygen toward Synergistic Catalytic Degradation of Tetracycline and *p*-Nitrophenol. *Sep. Purif. Technol.* **2024**, *329*, 125195. [CrossRef]
41. Zhang, Q.; Zuo, J.; Peng, F.; Chen, S.; Wang, Q.; Liu, Z. A Non-Noble Monometallic Catalyst Derived from Cu–MOFs for Highly Selective Hydrogenation of 5-Hydroxymethylfurfural to 2,5-Dimethylfuran. *ChemistrySelect* **2019**, *4*, 13517–13524. [CrossRef]
42. Chaminand, J.; Djakovitch, L.; Gallezot, P.; Marion, P.; Pinel, C.; Rosier, C. Glycerol Hydrogenolysis on Heterogeneous Catalysts. *Green Chem.* **2004**, *6*, 359–361. [CrossRef]
43. Tajvidi, K.; Pupovac, K.; Kükrek, M.; Palkovits, R. Copper-Based Catalysts for Efficient Valorization of Cellulose. *ChemSusChem* **2012**, *5*, 2139–2142. [CrossRef] [PubMed]